MODELING LANDSCAPE EVOLUTION DUE TO TILLAGE: MODEL DEVELOPMENT

D. A. N. Vieira, S. M. Dabney

ABSTRACT. *Tillage erosion has been identified as an important contributor to the modification of agricultural landscapes. A two-dimensional, grid-based model has been developed to compute soil redistribution and morphological changes of complex landscapes due to tillage operations. Soil movement along and perpendicular to the directions of tractor movement are computed as a function of local slope gradients and of characteristics of the tillage implement. A control volume approach is employed to determine terrain elevation changes after each tillage pass. The model explicitly considers the presence of internal and external field boundaries, simulating their influence on the development of erosion and deposition patterns. GIS layers are used to provide terrain elevation data, actual tillage directions, field borders, and the location of other features, such as vegetated strips, trees, or fences. The model was verified against an analytical solution for the development of bench terraces due to tillage between vegetated strips. The model's capability of considering variable tillage directions was tested with a simulation of tillage erosion over a synthetic, undulating surface and was used to investigate how an implement's forward and lateral soil displacement characteristics influence erosion patterns as a function of tillage direction relative to slope. The model's stability, computational efficiency, and ability to simulate fields with complex boundaries and varying tillage directions allow its use as a practical tool within a comprehensive conservation planning system.*

Keywords. *Landscape evolution, Mathematical models, Soil redistribution, Tillage erosion, Tillage translocation.*

Soil translocation and redistribution by tillage has been recognized as an important process in the morphological evolution of complex landscapes. Tillage erosion occurs because mechanical implements displace soil at rates that vary according to the terrain's slope gradient, and deposition or erosion occurs where there is a change in local soil displacement rates due to slope gradient changes or discontinuities. In complex landscapes, tillage erosion usually occurs on convexities, such as hilltops and knolls, and along upslope field borders (Schumacher et al., 1999), while deposition occurs in concave slope positions and at downslope fields edges. Locations mid-slope usually do not have important net erosion or deposition due to tillage, because the variation in slope gradients is small. The amount of soil displaced downhill by an implement is not entirely compensated by an operation in the opposite direction, thus creating a net movement of soil in the downhill direction. Due to gravity, more soil is also displaced laterally, in the downhill direction.

The importance of tillage erosion has been extensively documented. Although the displaced soil typically does not leave the field, erosion rates rival those of water erosion (Lindstrom et al., 1992; Lobb et al., 1995; Poesen et al., 1997), and observed patterns of total erosion and deposition are usually better explained when tillage erosion is accounted for (Lindstrom et al., 1990; Van Oost et al., 2000a, 2003).

The presence of physical boundaries such as field borders, fences, trees, and vegetative barriers, for example, creates discontinuities in the soil movement that lead to increased morphological changes. Boundaries are important for up- and downslope tillage as well as for contour tillage. Frequently, they are locations where tillage starts or stops, causing localized soil loss or accumulation. When tillage is performed parallel to a field border, accumulation is often observed due to soil displacements perpendicular to that direction, leading to the formation of tillage berms (Dabney, 2006). The introduction of an obstacle across a sloping, tilled field causes deposition to occur on the upslope side of it, while erosion happens on the downslope side. After years of repeated operations, tillage decreases the terrain slope gradients in the vicinity of the barrier, accelerating the formation of terrace benches, and the creation of positive or negative lynchets, or soil banks resulting from discontinuities in terrain elevation at each side of the barrier (Dabney et al., 1999; Papendick and Miller, 1977). Negative lynchets, where repeated operations have led to exposure of subsoil, can be detrimental to agricultural production.

Soil displacement caused by tillage is also important in the redistribution of soil constituents within the field (Sibbesen et al., 1985; Sibbesen, 1986; Van Oost et al., 2000b; Papiernik et al., 2005). Even if there is no erosion or deposition, each tillage operation moves large amounts of soil, and with it nutrients and possible contaminants sorbed to the soil. In areas of erosion, subsequent tillage operations incorporate nutrient-poor subsoil into the plow layer, which is then transported downslope, resulting in a plow layer with high variability of soil properties. Because the magnitude of trans–

Submitted for review in April 2008 as manuscript number SW 7448; approved for publication by the Soil & Water Division of ASABE in September 2009.

The authors are **Dalmo A. N. Vieira,** Research Hydraulic Engineer, and **Seth M. Dabney, ASABE Member,** Research Agronomist; USDA-ARS National Sedimentation Laboratory, Oxford, Mississippi. **Corresponding author:** Dalmo A. N. Vieira, USDA-ARS National Sedimentation Laboratory, P.O. Box 1157, 598 McElroy Drive, Oxford, MS 38655; phone: 662-232-2951; fax: 662-281-5706; e-mail: dalmo.vieira@ars.usda.gov.

location is considerable, soil properties can be significantly affected after only a few tillage operations.

Although several models have been proposed and successfully applied to a variety of situations (Lobb and Kachanoski, 1999; Lindstrom et al., 2000; Van Oost et al., 2000a; De Alba, 2001, 2003; Li et al, 2007a), there is still a need for a computer model to predict morphological changes that result from the complex soil displacements that occur on a cultivated field and that specifically accounts for the presence of physical barriers, because it is in their vicinity that the most important morphological changes take place.

Several models disregarded the direct effects of physical boundaries on the process of erosion, limiting the analysis to interior areas. De Alba (2003) reported instabilities near boundaries, so that the area within 6 m from a boundary was artificially leveled. Li et al. (2008) established a 5 m wide buffer zone in which terrain elevations were adjusted so that the terrain slope gradually approached zero. Other models employed simplified boundary conditions that may not reflect realistically the conditions observed during real tillage operations in agricultural fields, such as holding constant terrain elevation and slope (e.g., Lindstrom et al., 2000).

Our objective in this study was to develop and validate a two-dimensional, grid-based computer model that simulates the evolution of complex landscapes due to tillage, considering the interactions between topography, paths and directions taken by tillage implements, and the presence of geometrically complex boundaries and obstacles. The model is intended to serve as a field-scale conservation planning tool that can be applied to actual field configurations in a GIS context.

Theory of Soil Translocation

Because of some confusion in the literature concerning the way tillage erosion is calculated, we provide the following summary of previous approaches as an introduction to the exposition of our model. Tillage erosion was recognized as an important factor in the development of landscapes in cultivated areas as early as the early 1940s, when tests were conducted to estimate soil translocation for several implements (Mech and Free, 1942). It was not until the 1990s, however, that the subject was studied in more detail. Lindstrom et al. (1990, 1992) measured soil movement from moldboard plowing and disking, and showed that the amounts of soil translocated, both in the direction of tillage and in the direction perpendicular to it, were directly proportional to the slope gradient (fig. 1).

In figure 1, the slope gradient *s*, the tangent of the slope angle, is taken as positive when tillage progresses upslope, and negative when tillage is in the downslope direction. The translocation distance can be expressed as:

$$d = a + bs = a + b\frac{\partial z}{\partial r} \tag{1}$$

where *d* is the mean translocation distance of the plow layer, *s* is the slope gradient, *a* and *b* are the regression coefficients, and the slope gradient is approximated by the derivative $\partial z / \partial r$, where *z* is the local terrain elevation and *r* indicates the direction in which the translocation distance is being

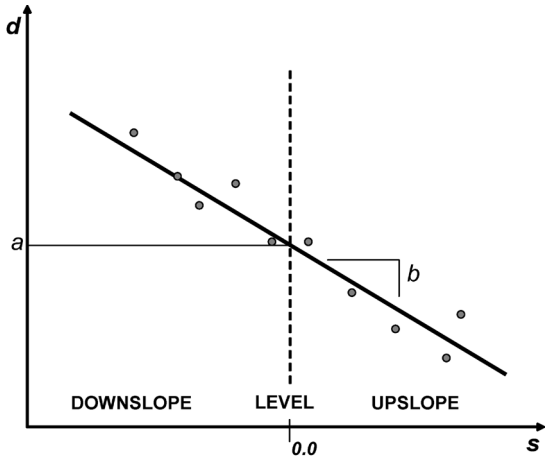

Figure 1. Typical plot of tillage translocation distance (*d*) versus slope gradient (*s*), for each tillage pass. Upslope gradient is positive slope; downslope gradient is negative.

evaluated. The coefficient *a* represents the translocation amount that occurs when the slope in the direction of *r* is zero. Following Lindstrom et al. (1990), the coefficient *b* is negative so that downslope translocation is positive.

Extending the initial development of Lindstrom et al. (1990, 1992), Govers et al. (1994) also utilized equation 1 to develop a model to compute terrain elevation changes using the one-dimensional conservation of mass equation for sediment movement on a hillslope:

$$\rho_b \frac{\partial z}{\partial t} = -\frac{\partial Q_s}{\partial r} \tag{2}$$

where ρ_b is the bulk density of the soil, *z* is the terrain elevation, Q_s is the soil mass flux (mass per unit width per tillage operation) in the *r*-direction, and *t* is time. In this context, *t* can be seen as a number of tillage passes, and $\partial z / \partial t$ is the corresponding terrain elevation change. The mass flux can be estimated from the measured average soil displacement of the plow layer (*d*), if the depth of tillage *D* and the bulk density are known:

$$Q_s = \rho_b D d \tag{3}$$

For up- and downslope tillage, assuming the *r*-axis to be positively oriented in the downslope direction, the mass fluxes, expressed in units of mass per unit width, can be written as:

$$Q_{DN} = \rho_b D d_{DN} \tag{4a}$$

$$Q_{UP} = -\rho_b D d_{UP} \tag{4b}$$

where Q_{DN} and Q_{UP} are the mass fluxes, and d_{DN} and d_{UP} are the translocation distances for tillage in the downslope and upslope directions, respectively. Govers et al. (1994) assumed one tillage operation per year and that successive tillage operations take place in opposing directions, so that the average net downslope flux per unit width per year could be written as:

$$Q_s = \frac{Q_{DN} + Q_{UP}}{2} = \frac{\rho_b D\left(d_{DN} - d_{UP}\right)}{2} \tag{5}$$

Utilizing equation 1 to correlate the soil translocation to the slope gradient, we have:

$$Q_s = \frac{\rho_b D}{2}\left[a + b\frac{\partial z}{\partial r} - \left(a + b\left(-\frac{\partial z}{\partial r}\right)\right)\right]$$

$$= \rho_b D b \frac{\partial z}{\partial r} \quad (6)$$

Note that Q_s is positive because b is always negative with the convention used here, and $\partial z/\partial r$ is negative downslope. Equation 6 can be rewritten as:

$$Q_s = -k\frac{\partial z}{\partial r} \quad (7)$$

where k, a positive number (kg m^{-1}), is given by:

$$k = -\rho_b D b \quad (8)$$

Using equations 7 and 2, we get:

$$\rho_b \frac{\partial z}{\partial t} = k\frac{\partial^2 z}{\partial r^2} \quad (9)$$

which shows that the process of erosion due to tillage can be represented by a diffusion-type equation, valid for the assumption of two successive operations in opposite directions, without modification of terrain slopes after the first operation takes place.

Lobb and Kachanoski (1999) proposed that the tillage translocation, expressed in mass per unit width per tillage pass, could be related to the slope gradient S, given as a percentage and positive in the downslope direction:

$$Q_s = \alpha + \beta S \quad (10)$$

The coefficient α represents the translocation amount unaffected by terrain slope or curvature, while β (kg m^{-1} %$^{-1}$ pass^{-1}) represents the effect of slope gradient on the amounts of displaced soil. It is important to note the distinction between coefficients α and β, which relate to translocation mass, and coefficients a and b in equation 1, which relate to translocation distance.

It is possible to deduce the relationship between tillage coefficient k (Govers et al., 1994) and coefficient β (Lobb and Kachanoski, 1999) with the following reasoning. Starting from the expression that relates translocation mass and translocation distance (eq. 3) and using the correlation of translocation distance with slope (eq. 1) with the slope expressed as a percentage, positive in the downhill direction, we get:

$$Q_s = \rho_b D d = \rho_b D\left(a - b\frac{S}{100}\right) \quad (11)$$

Equating equation 11 to equation 10, and introducing the definition of k (eq. 8), we get:

$$\alpha + \beta S = \rho_b D a + k\frac{S}{100} \quad (12)$$

When the terrain slope is zero, the soil translocation in mass per unit width relates to the translocation distance through the relation $\alpha = \rho_b D a$. Therefore, from equations 12 and 8, we conclude that:

$$\beta = \frac{k}{100} = -\frac{\rho_b D b}{100} \quad (13)$$

Other researchers also searched for similar relationships. Lobb and Kachanoski (1999) also proposed an equation relating soil translocation to the slope gradient S and curvature φ (% m^{-1}):

$$Q_s = \alpha + \beta S + \gamma\varphi \quad (14)$$

where γ is a regression coefficient (kg m^{-1} (%$^{-1}$ m)$^{-1}$ pass^{-1}). The inclusion of the slope curvature term in equation 14 improves the description of measured translocated mass, but equation 10 is capable of predicting tillage translocation with similar performance (Li et al., 2007b). De Alba (2001, 2003), for example, developed a relationship based on measurements for a moldboard plow in which the soil displacement is also correlated to the slope steepness in the lateral direction. Quine and Zhang (2004) questioned the applicability of Lindstrom's linear equation for upslope tillage, and proposed a relationship using an oblique slope, derived from moldboard plow data. Heckrath et al. (2006) developed displacement functions using second-degree polynomials, also based on moldboard plow experiments. For the present model, however, it is believed that expressing soil translocation in mass per unit width per tillage operation as a function of the slope gradient (eq. 10) is the best choice. The same equation can be used for estimating soil translocation in the direction of tillage and in the direction perpendicular to it. The ability of computing translocations in orthogonal directions separately is an advantage in the mathematical formulation of the model being proposed. In addition, this type of translocation relationship can be employed for any tillage implement, and the regression coefficients can be easily obtained from translocation measurements.

Tillage Erosion and Landscape Evolution Model

The terrain is described by a two-dimensional grid of uniform-size cells (a digital elevation model, or DEM) at a resolution fine enough to characterize its topography. Tillage directions are also defined for each cell as azimuth angles. Figure 2 shows the computational grid, where nodes at the centroids of the control volumes define the location where soil translocation rates and terrain elevation changes are computed. For each cell, soil translocation caused by the tillage implement is computed with equation 10 using local slope gradients; the equation is applied separately for translocation in the direction of tillage and in the direction perpendicular to it. The total translocation at a node is the vectorial sum of components computed separately in two orthogonal directions. The soil fluxes crossing each cell face are then determined, and the principle of conservation of mass, applied to each computational cell, determines terrain elevation changes after each tillage pass, with the assumption that temporal changes in bulk density can be neglected. Therefore, changes in topography are immediately reflected on the slope gradients computed for the subsequent tillage pass.

This formulation facilitates the development of numerical procedures because it allows the mathematical treatment of soil fluxes as vectorial quantities. The method also accounts for the presence of field borders and barriers that stop or limit

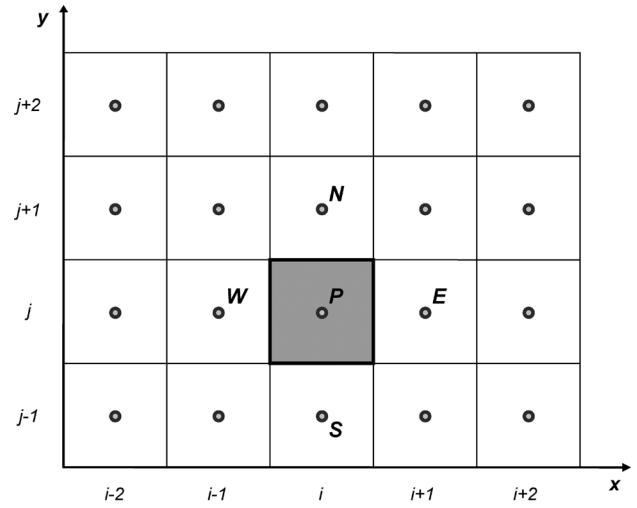

Figure 2. Cell-centered finite volume 2D grid. A node at the center of each cell represents the location where terrain elevations and tillage directions are given, and where soil translocation and erosion or deposition are computed.

soil movement. The position of these features is adjusted to coincide with the faces of computational elements to facilitate the specification of boundary conditions (soil fluxes through the cell faces) for the conservation of mass equation.

The grid may cover a region larger than the area of tillage, or encompass more than one agricultural field. The specification of field boundaries combined with tillage information permits several fields in the same DEM to be simulated at once. The adoption of a structured grid increases computational efficiency, while the use of fine spatial resolution, in the range of 1 to 5 m, is adequate for the positioning of boundaries for consideration of actual tillage directions, which may follow curvilinear paths, as in the case of contour tillage. A grid-based approach also facilitates the specification of input data using GIS software for preprocessing and data preparation.

Numerical Approach

The numerical solution approach exploits the fact that soil fluxes are vectorial quantities, and that tillage direction determines the local effective slopes (in the directions of tillage and normal to it) and the consequent magnitude of soil translocation. The domain is subdivided into small rectangular, non-overlapping cells by a structured grid that defines the control volumes' boundaries. The Cartesian directions *x* and *y* are assumed parallel to the DEM borders. The solution method utilizes a cell-centered finite volume approach to determine elevation changes at each cell using the principle of conservation of mass. Soil crosses each of the four cell faces at different rates, resulting in change of terrain elevation. The main advantage of this discretization method is that the resulting solution satisfies conservation of mass exactly for any control volume as well as for the whole simulation domain (Ferziger and Perić, 1999).

The conservation of mass in integral form can be written for a finite control volume *CV* with a bounding control surface *CS* as (Ferziger and Perić, 1999):

$$\frac{\partial}{\partial t}\int_{CV} \rho_b dV + \oint_{CS} \rho_b(\vec{v}\cdot\vec{n})dS = 0 \qquad (15)$$

where the first term represents the time rate of change of the total mass inside the finite control volume, and ρ_b is the soil density. The mass flux of soil through a surface fixed in space is given by the second term, where $\vec{v}$ is the velocity component perpendicular to the elemental surface area *dS*, and $\vec{n}$ is its associated, outward-pointing unit normal vector. In the case of tillage erosion, $\vec{v}$ is the soil displacement for a tillage operation. An algebraic equation can be obtained through formulas that approximate the volume and surface integrals. A two-dimensional, Cartesian control volume arrangement is established according to figure 3a. Each *CV* has a central node *P*, and its surface is represented by four planar faces (*e*, *w*, *n*, *s*) separating it from neighboring cells, referred to by the cardinal points (*E*, *W*, *N*, *S*).

Because ρ_b is constant within the *CV*, whose area does not change in time, the change in elevation z_P can be obtained

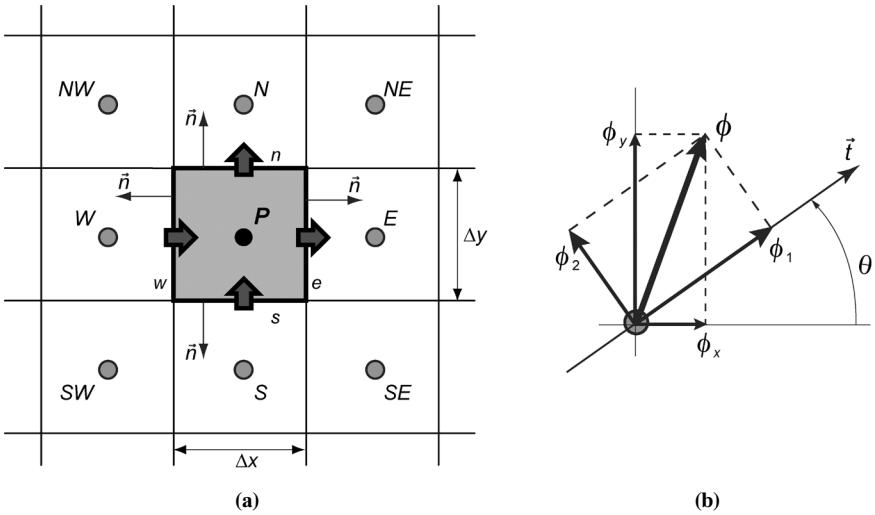

Figure 3. (a) Computational control volume. Point *P* is at the center of the cell, where properties are computed. Arrows indicate soil fluxes across the four cell faces. (b) Tillage translocation vectors. The total net translocation vector ϕ is the sum of its components ϕ_1 and ϕ_2, computed in the direction of tillage $\vec{t}$ and perpendicular to it, respectively. The same vector can be represented by its components in the Cartesian directions (ϕ_x and ϕ_y), which are used to determine the soil fluxes through the cell faces, from which elevation changes for the cell are computed using a mass balance equation.

directly from the term representing the time rate of change of mass M:

$$\frac{\partial}{\partial t}\int_{CV}\rho_b dV = \frac{\partial(\rho_b V)}{\partial t} = \frac{\partial M}{\partial t} = \rho_b A\frac{\partial z_P}{\partial t} \qquad (16)$$

where A is the surface area of the control volume.

The surface integral of equation 15 is substituted by the sum of integrals along each of the four faces that define the bounding contour surface CS. For the finite CV, $\vec{n}$ represents the outward normal to each of its faces. The flux of soil through each face is approximated by the product of the flux at the cell face center (in itself an approximation of the mean value over the face) and the cell face area. For each face:

$$\Phi = \oint_{CS}\rho_b(\vec{v}\cdot\vec{n})dS = \rho_b\overline{d}\,\overline{D}\Delta = \phi\Delta \qquad (17)$$

where Φ is the mass flux in units of mass per tillage operation, and $\overline{d}$ and $\overline{D}$ are the average soil displacement and tillage depth at the face of size Δ. The mass flow rate per unit width perpendicular to each cell face, ϕ, is obtained through linear interpolation from values estimated at nodes to each side of the cell face.

The conservation of mass equation can then reduce to $\rho_b A\,\partial z_P/\partial t - \Phi_w + \Phi_e - \Phi_s + \Phi_n = 0$. The negative signs for the west and south faces result from the convention used for the integration path: the outward normal vectors for those faces (fig. 3a) are in opposite directions to those for the east and north faces, and to the orientation of the Cartesian axes. In the present case, time refers to a single tillage pass, and $\partial z_P/\partial t = \Delta z_P = z_P^{n+1} - z_P^n$ is the resulting elevation change. For a typical control volume, the new elevation after a single tillage pass is given by:

$$z_P^{n+1} = z_P^n + \frac{\Phi_w - \Phi_e + \Phi_s - \Phi_n}{\rho_b \Delta x \Delta y} \qquad (18)$$

where Δx and Δy are the cell sizes in the x and y directions.

Soil Translocation

The soil mass fluxes through the control volume faces result from the translocation caused by tillage equipment. The magnitude of soil translocation forward in the direction of tillage (ϕ_1) and laterally, perpendicular to the tillage direction (ϕ_2), in mass per unit width, can be estimated using the relationship proposed by Lobb and Kachanoski (1999), (eq. 10):

$$\phi_1 = \alpha_1 + \beta_1 S_1 \qquad (19a)$$

$$\phi_2 = \alpha_2 + \beta_2 S_2 \qquad (19b)$$

where α_1 is the net translocation amount in the tillage direction, in kilograms per meter width, per tillage operation on level ground; β_1 is the slope-effect coefficient, characteristic of the tillage implement, in kilograms per meter width of tillage per % slope gradient; and S_1 is the slope gradient (%) in the tillage direction. Similarly, equation 19b refers to soil movement in the lateral direction, identified by the subscript 2. The coefficient α_2 is the net soil translocation in the lateral direction, positive for net displacement to the right. Symmetric (two-way) implements operating on level ground displace soil laterally at equal rates, therefore $\alpha_2 = \alpha_{right} - \alpha_{left} = 0$. A database of translocation coefficients for a variety of tillage implements obtained from field measurements is available from the published literature (Lobb et al., 1995, 1999; Van Muysen et al., 2000, 2002; Van Muysen and Govers, 2002; Da Silva et al., 2004; Heckrath et al., 2006; Tiessen et al., 2007a, 2007b; Li et al., 2007b).

The slope gradients S_1 and S_2 in the tillage and normal-to-tillage directions are computed for each cell based on the elevation data:

$$S_1 = \vec{t}_1 \cdot \vec{\nabla}_z \qquad (20a)$$

$$S_2 = \vec{t}_2 \cdot \vec{\nabla}_z \qquad (20b)$$

where $\vec{t}_1$ and $\vec{t}_2$ are unit vectors defining the two directions, and the gradient is given by:

$$\vec{\nabla}z = \left(\frac{\partial z}{\partial x}, \frac{\partial z}{\partial y}\right) = \frac{\partial z}{\partial x}\vec{i} + \frac{\partial z}{\partial y}\vec{j} \qquad (21)$$

where $\vec{i}$ and $\vec{j}$ are unit vectors along the x and y axes, respectively.

Tillage Directions and Slope Gradients

In order to allow for a realistic representation of tillage operations, each CV has a potentially different tillage direction, specified by an azimuth A in degrees, according to the usual geographic convention (A = 0 indicates north, increasing in the clockwise direction). For computation of the directional slopes, the tillage direction is converted to degrees using the trigonometric convention, through the relationship:

$$\begin{cases}\theta = 90° - A & 0° \le A \le 90° \\ \theta = 450° - A & 90° < A < 360°\end{cases} \qquad (22)$$

and the directional slopes are computed using:

$$S_1 = \cos\theta\frac{\partial z}{\partial x} + \sin\theta\frac{\partial z}{\partial y} \qquad (23a)$$

$$S_2 = \sin\theta\frac{\partial z}{\partial x} - \cos\theta\frac{\partial z}{\partial y} \qquad (23b)$$

The computation of the terrain slope terms $\partial z/\partial x$ and $\partial z/\partial y$ is a very important aspect of the tillage erosion computation. Several algorithms for slope calculation are available in the literature (Sharpnack and Akin, 1969; Fleming and Hoffer, 1979; Horn, 1981; Ritter, 1987). Jones (1998a, 1998b) evaluated eight of these methods using synthetic, analytically defined DEMs with various amounts of added noise, and showed that methods using elevation values in a 3 × 3 window, or kernel, were considerably more accurate than simpler methods that did not. For non-smooth surfaces, typical of natural terrains, the method of Horn (1981) proved to be one of the best. Horn's method, also reported by Burrough and McDonnell (1998), is a method commonly employed by GIS software and was selected for this program. Horn's method utilizes a 3 × 3 moving kernel (fig. 3a) to evaluate the first derivatives of elevation (slope gradients) using a central difference scheme. Slope gradients evaluated at the CV's central node P are given by:

$$\frac{\partial z_P}{\partial x} = \frac{(z_{NE} + 2z_E + z_{SE}) - (z_{NW} + 2z_W + z_{SW})}{8\Delta x} \quad (24a)$$

$$\frac{\partial z_P}{\partial y} = \frac{(z_{NW} + 2z_N + z_{NE}) - (z_{SW} + 2z_S + z_{SE})}{8\Delta y} \quad (24b)$$

Error statistics determined for the estimation of slope gradients with the above equations show that a more accurate representation of a continuous terrain is obtained if grid cells are smaller (Jones, 1998a), that in general complex terrain is less accurately represented than a simple terrain at the same resolution level, and that the accuracy of slope representation is more sensitive to resolution reduction for a complex terrain than a simple terrain (Tang et al., 2003).

For cells at the boundaries of the simulation domain or adjacent to internal boundaries, where one or more neighbor elevation points may not be available, equations 24a and 24b are still used, but linear interpolation is employed to estimate the elevation values of the missing nodes. Figure 4 illustrates how interpolations are made for a cell at a boundary corner. Nodes NW, W, SW, S, and SE are beyond the boundary; hence, their values are unavailable for the estimation of slope gradient. The elevation of a node beyond a field boundary (indicated in the figure as "ghost" cells, shown in dashed lines) is determined using the slope gradient in the direction perpendicular to the boundary, computed from terrain elevation values for points inside the simulation domain. The terrain elevation for point SW is set as the average of estimates computed using slope gradients in orthogonal directions.

Soil Mass Fluxes

The soil translocations in the tillage and lateral directions, computed by equations 19a and 19b, are then combined and projected into the *x* and *y* Cartesian directions, as illustrated in figure 3b, using the following relationships:

$$\phi_x = \phi_1 \cos\theta + \phi_2 \cos(\theta - 90°) \quad (25a)$$

$$\phi_y = \phi_1 \sin\theta + \phi_2 \sin(\theta - 90°) \quad (25b)$$

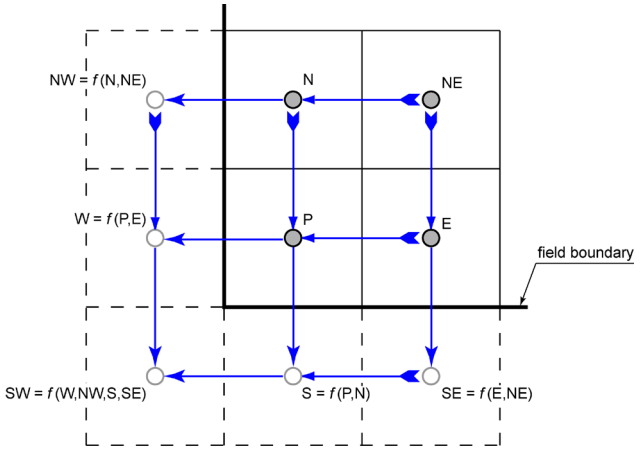

Figure 4. Computation of slope gradients for cells adjacent to boundaries. Elevation for point NW is estimated from slope gradient computed with points N and NE; similarly for points W, S, and SE. For corner point SW, elevation is set as the average of elevations interpolated from points NW-W, and SE-S.

These values, computed for the nodes at the center of each cell, are the components of soil translocation (in units of mass per unit width, per tillage operation) in the Cartesian directions. The mass of soil traversing each cell face, located midway between cell centers, is obtained from the product of the mass flux per unit width normal to that face (obtained by interpolation from the nodal values) and the cell face length:

$$\Phi_w = \frac{(\phi_{x_{i-1,j}} + \phi_{xi,j})}{2}\Delta y \quad (26a)$$

$$\Phi_e = \frac{(\phi_{x_{i+1,j}} + \phi_{xi,j})}{2}\Delta y \quad (26b)$$

$$\Phi_s = \frac{(\phi_{y_{i,j-1}} + \phi_{y_{i,j}})}{2}\Delta x \quad (26c)$$

$$\Phi_n = \frac{(\phi_{y_{i,j+1}} + \phi_{y_{i,j}})}{2}\Delta x \quad (26d)$$

The amount of soil leaving one cell matches exactly the amount entering a neighboring cell through a common cell face, thus ensuring conservation of mass. Once the mass fluxes through each cell face are computed, equation 18 is used to compute new terrain elevations after each tillage pass.

Field and Internal Boundaries

For cells at the boundaries of the simulation domain or adjacent to a field border or other barriers, proper boundary conditions must be prescribed. In the model, boundaries must coincide with the location of the *CV* faces, and boundary conditions are applied separately to each face. A model's boundary condition is an approximation of a physical situation, and it should represent what happens in nature. In tillage erosion modeling, prescription of boundary conditions is important because boundaries exert a large influence on the processes of soil loss and accumulation. It is common to find situations where the greatest changes occur near boundaries.

Two classes of boundary conditions are used to define the model limits and to describe how the presence of a physical boundary affects local soil displacement and triggers localized soil erosion or deposition:

A "closed" boundary condition, perhaps the most evident type, enforces in the computations the situation where no soil traverses the face where the condition is applied. This is the type used for high field berms or very dense or impenetrable vegetative barriers, for example, where it can be assumed that the amount of soil that crosses the boundary is negligible. Numerically, it consists of simply setting the flux across the corresponding faces of all *CV*s along the boundary to zero ($\phi_{\vec{n}} = 0$). This type of boundary condition leads to either deposition or erosion in the computational cell where it is applied, depending on the direction of the component of the soil flux normal to the boundary. If the soil is moving away from the boundary, then soil loss occurs; otherwise accumulation occurs.

An "open" boundary condition allows the soil to cross the *CV* face at a rate and direction equal to the rate computed for

the opposite face of the same CV ($\partial\phi/\partial\vec{n} = 0$). This type of condition is useful when simulating an "open-ended" domain, where no physical boundary exists. Practical applications of this type of boundary condition include situations where tillage extends beyond the model boundaries, or when the exact location where tillage starts and stops is unknown. It can also be used when tillage boundaries vary between operations. This condition is useful because it does not let the presence of the boundary influence the soil movement inside the simulated region. There is no localized erosion or deposition near the boundaries when this condition is used. Soil flows out of the simulation domain if the computed soil flux is toward the boundary. Conversely, soil enters the field if the computed soil flux is directed away from the boundary.

Program Implementation and Required Input Data

The numerical procedure described above has been implemented into a computer program using Fortran 95. The program has been designed to be used as a stand-alone simulation program or as a component of a more complete landscape evolution model. Input data consist of three parts: initial elevations in the form of a DEM covering the area to be simulated, location of field borders and internal boundaries, and tillage operation data. The program contains a series of preprocessing routines that simplify its use. Among the most important are the automatic definition of which DEM cells will in fact become control volumes inside the simulation domain, the setup of boundary conditions, and the management of tillage data.

The resolution used for the numerical solution is the same resolution as the DEM that supplies the initial elevations used in the simulation. Tilled areas to be simulated, as well as areas of exclusion (e.g., ponds, vegetated areas), are provided as polygons, digitized with the help of a GIS program. Linear features to be considered as internal boundaries, such as fences, grass hedges, and other barriers, are delineated in a similar manner. A series of computational geometry algorithms, borrowed from the field of computer graphics (Schneider and Eberly, 2002), decide which DEM cells belong to the simulation domain, and then for each *CV*, what faces require a particular boundary condition. Boundary lines are adjusted to coincide with the closest computational cell faces, and lines deviating from east-west or north-south directions are represented by a staircase pattern, as illustrated in figure 5.

Tillage data are provided to the model through one or more "tillage pattern" raster files, which contain tillage directions (azimuths) for each cell in the computational domain, and a single XML (extensible markup language) file that describes implement characteristics and tillage operations. This "tillage operations" file contains two basic data sections: implement descriptions, and management sequences. The implement descriptions section specifies each implement type, an ID code, and the tillage translocation coefficients that characterize its erosivity. The management sequences section describes the dates when operations are performed and is used to control the execution of the simulations. Each sequence may have one or more tillage operations, each comprised of a prescribed number of passes by a certain implement; tillage passes can alternate directions or not. An operation uses tillage patterns provided in the separate raster files. The tillage pattern files are created in a preprocessing step where GIS algorithms are used to analyze a layer with a series of lines defining paths and directions taken by the tillage implements.

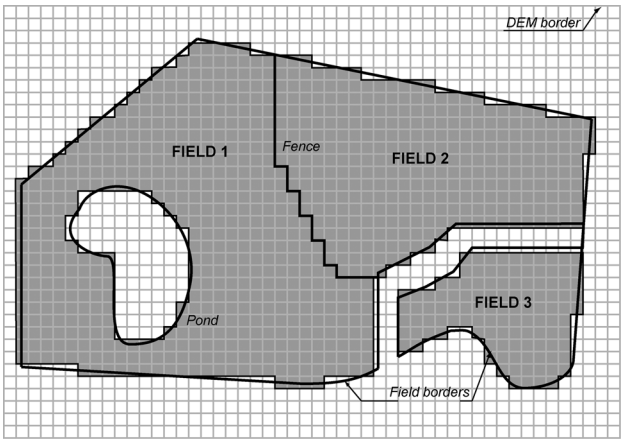

Figure 5. Approximation of internal and external field boundaries with a regular grid. Lines indicate field borders or obstacles such as vegetated strips or fences. Shaded cells belong to the computational domain.

Model Verification

For any numerical model, it is necessary to verify that the model assumptions and formulations represent well the physical phenomena, and that the computer code is free of errors or inconsistencies. In the case of the tillage erosion model, new terrain elevations are computed using a time-marching procedure. For each time step, corresponding to a tillage pass, terrain elevations changes are obtained using the principle of conservation of mass within a computational cell. The soil mass fluxes across the faces of such cell result from estimates of soil translocation based on local slope gradients. Therefore, it is important to verify that (1) the simulation domain is discretized into computational cells adequately, (2) terrain topography and tillage directions are well prescribed, (3) boundary conditions are properly enforced, (4) terrain slope gradients are correctly computed, and (5) soil mass fluxes and the resulting erosion or deposition are calculated accurately.

It is convenient to test the model for idealized situations for which analytical solutions may be available, because: (1) the process of tillage erosion is highly variable and it occurs over many years, and (2) it is very difficult to separate tillage erosion from water and wind erosion. At the same time, it is important to apply the tillage model to a configuration that represents well the process of tillage erosion over complex landscapes and to test its performance near boundaries that interrupt or modify soil displacement. It is also beneficial to simulate a situation that occurs routinely in agricultural fields, as the model application can provide insight into the process of tillage erosion itself.

Dabney et al. (1999) documented the process of formation of bench terraces created by contour tillage between vegetative barriers. Bench terraces are embankments built along the contour of a sloping land with the purpose of controlling runoff and erosion. Soil translocation caused by

tillage creates patterns of soil erosion and deposition that decrease slope steepness and promote the development of terrace benches. Terrain elevation changes along a profile can be described by the one-dimensional diffusion equation (eq. 9):

$$\frac{\partial z}{\partial t} = K \frac{\partial^2 z}{\partial x^2} \tag{27}$$

where $K = 100\beta/\rho_b$ (see eq. 13), and β is the soil translocation coefficient related to the slope gradient in the direction perpendicular to the boundary.

Let us consider a section of an agricultural field limited on both sides by closed boundaries, separated by a distance L, which are assumed to completely prevent the passage of soil. We also assume that the terrain is initially planar and with a slope gradient of s. For tillage in alternating directions, the zero-flux condition at the boundaries is analogous to the Neumann boundary condition $\partial z/\partial x = 0$, and the problem can be formulated as:

$$\begin{cases} \partial z/\partial t = (100\beta/\rho_b)\,\partial^2 z/\partial x^2 & \\ z(0,x) = sx & 0 \le x \le L \\ \partial z/\partial x\,(t,0) = \partial z/\partial x\,(t,L) = 0 & 0 \le t \le \infty \end{cases} \tag{28}$$

The solution for the problem can be obtained through the method of separation of variables (e.g., Boyce and DiPrima, 1977). Terrain elevation values at any point in time and space can be obtained from the infinite series given by:

$$z(t,x) = \frac{A_0}{2} + \sum_{n=1}^{\infty} \left(A_n \cos\left(\frac{n\pi x}{L}\right) e^{-K\left(\frac{n^2\pi^2}{L^2}\right)t} \right)$$
$$n = 1,2,3... \tag{29a}$$

where

$$A_0 = \frac{2}{L}\int_0^L sx\,dx \tag{29b}$$

$$A_n = \frac{2}{L}\int_0^L sx \cos\left(\frac{n\pi x}{L}\right) dx \tag{29c}$$

The two-dimensional tillage model was used to compute the process of landscape benching due to contour tillage for a stretch of cropland between grass hedges 20 m apart (fig. 6), which is similar to the field described by Dabney et al. (1999). In the simulation, the slope gradient in the direction perpendicular to the hedges was set at $s = 0.15$ m m^{-1}, and the field was discretized using square cells 0.5 × 0.5 m. For cell faces bordering the grass hedges, a "closed" boundary condition was specified, enforcing the assumption that no soil will cross the hedges. For the cell faces at the remaining field borders, an "open" boundary condition was prescribed to simulate an infinitely long field in the direction of the grass hedges. Tillage was assumed parallel to the hedges in alternating directions, for a total of 100 operations. Tillage in alternating direction is a requirement so that equation 27 can be used to represent the erosion process. A tillage implement that produces substantial lateral soil movement, such as a moldboard plow, was used. The values of the translocation coefficients prescribed for this simulation are given in table 1.

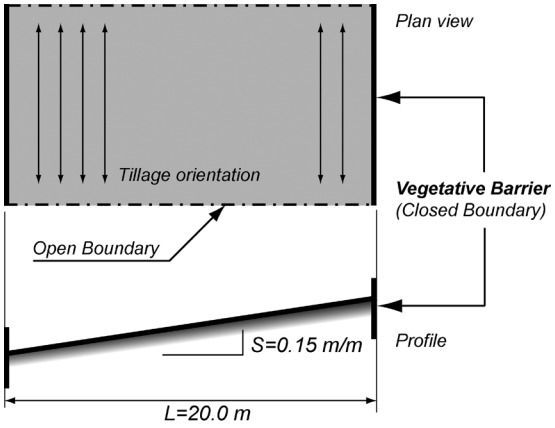

Figure 6. Field bordered by vegetative barriers. Boundaries where vegetative barriers are located are assumed to be completely closed.

Table 1. Soil and tillage implement properties.

Property	Symbol	Value
Soil translocation in the tillage direction on level ground	α_1	50.0 kg m^{-1} pass^{-1}
Slope gradient coefficient in the tillage direction	β_1	3.0 kg m^{-1} %$^{-1}$ pass^{-1}
Soil translocation in the lateral direction on level ground	α_2	25.0 kg m^{-1} pass^{-1}
Slope gradient coefficient in the lateral direction	β_2	1.5 kg m^{-1} %$^{-1}$ pass^{-1}
Soil bulk density	ρ_b	1500 kg m^{-3}
"Diffusion" coefficient	K	$100\beta_2/\rho_s = 0.1$

Note that the process of erosion and landscape evolution is controlled only by the slope gradient and the term $K = 100\beta_2/\rho_b$ in equation 28. Here, β_2 is the soil translocation coefficient related to the slope gradient, in the lateral direction, and thus normal to the grass hedge. The magnitudes of coefficients α_1, α_2, and β_1 do not affect erosion or deposition rates near the boundaries, as tillage in alternating direction cancels their effects.

Figure 7 shows the computed terrain elevations for a typical profile in the region across the grass hedges, after 50, 100, and 200 tillage passes. Model results are compared to the analytical solutions, given by equation 29, computed with a 500-term series expansion. After 200 operations, the maximum erosion and deposition is 0.75 m, near the grass hedges. Slope gradients near the center of the cropland reduce from 15% to 11.6%, while near the grass hedges the land slopes reduce to only 0.4%. Over the whole simulation domain, good agreement can be observed between the simulated results and the analytical solutions. These results verify that the numerical scheme was implemented well, as it reproduces the analytical solution. It is important to note that cells adjacent to the field borders also display a correct behavior: all computed properties are free of discontinuities, oscillations, instabilities, or any other defects. The numerical solution does not require any type of smoothing procedure or other artificial treatment. Computing time for a simulation domain of 1600 cells and 200 tillage passes takes less than 2 s on a computer with an AMD Athlon FX-62 processor.

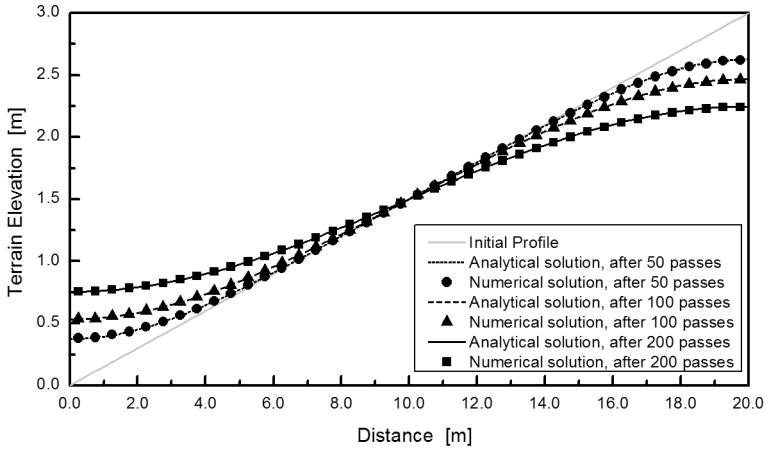

Figure 7. Comparison of model predictions and analytical solutions for landscape changes due to contour tillage. Terrain elevations after 50, 100, and 200 tillage passes.

In order to investigate how mesh size affects the accuracy of the model's solution, the same problem was solved in a longer slope with boundaries 100 m apart, allowing the use of meshes with different resolutions. Figure 8a shows the predicted terrain elevations after 100 tillage passes, computed with different mesh sizes. For clarity, the figure shows only part of the simulation domain, the first 20 m near the boundary at the slope bottom where deposition occurred. The markers indicate the location of computational nodes for simulations with different node spacings. The simulations show that the numerical approximation is convergent, that is, errors with respect to the exact solution become smaller as the mesh is refined. Root mean squared errors, computed using only nodes in the area of deposition, are 0.022, 0.011, 0.004, and 0.003 m for meshes with cell sizes 5.0, 2.0, 1.0, and 0.5 m, respectively. The results indicate that numerical errors can be controlled by sufficiently fine discretization.

The use of higher mesh resolution allows the model to describe fine-scale terrain features, and it is especially important near the boundaries, where the gradual process of erosion (or deposition) continuously reduces slope gradients, causing the area of morphological changes to be gradually increased. However, very fine mesh sizes are not desirable because they can lead to the computation of excessive erosion or deposition for cells adjacent to closed boundaries, where a large mass of soil is translocated in a computational cell of small dimensions, resulting in significant terrain elevation changes per tillage pass. A practical lower limit for

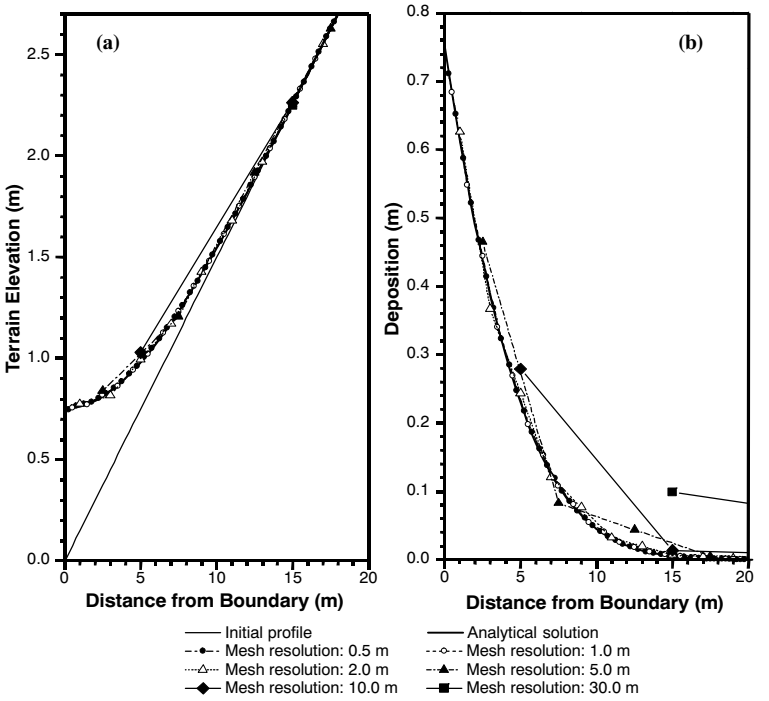

Figure 8. (a) Computed terrain elevations and (b) deposition near the downslope boundary for different mesh resolutions. Agreement between computed results and analytical solution improves through successive mesh refinements.

cell sizes is associated with the soil translocation distance. From equations 3 and 10, we can estimate the maximum computed translocation distance for the present test to be $d = (\alpha + \beta S) / (\rho_b D) = 0.32$ m, assuming a tillage depth $D = 0.10$ m. Using mesh sizes greater than the translocation distance d is therefore recommended.

Interactions between Tillage Direction and Topography

When tillage equipment passes over complex topography, the direction of maximum translocation may not coincide with the direction of tillage. Although the general effect of tillage is the filling of depressions and the erosion of slope convexities, it is interesting to know the actual directions of soil movement. In order to demonstrate how soil displacements change with tillage direction, we applied our model to a hypothetical concave terrain with varying slope gradients, shown in figure 9. A single computational cell with face size of 1.0 m is considered in a terrain with variable slope gradient along the y-axis and zero slope gradient in the x-direction. This configuration simplifies the identification of on-contour and up- and downslope tillage situations, and helps the visualization of the differences for intermediate directions. Soil translocation amounts and the resulting erosion or deposition were computed for varying tillage directions and for different tillage implements.

The terrain slope gradients in the x and y directions are given at point P, which characterizes soil translocation within the cell. For a given tillage direction, expressed as the angle θ measured counterclockwise from the x-axis, soil translocations in the direction of tillage and perpendicular to it are computed with equations 19a and 19b. The total translocation amount, the soil mass fluxes along the Cartesian axes, and the direction of maximum translocation

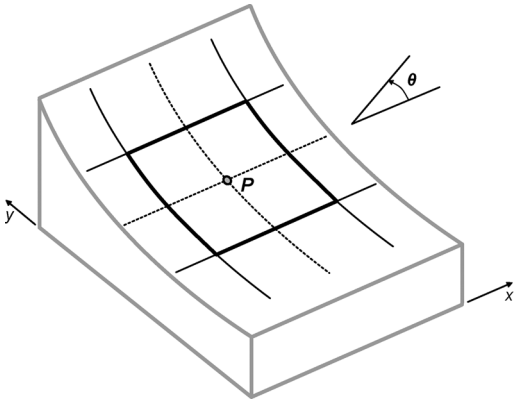

Figure 9. Computational cell in a concave slope of varying steepness.

are also computed. Erosion or deposition amounts are then estimated using equation 18.

The terrain slope gradient at the center of the computational element (point P) is 10%, varying with a curvature (along y) of 0.025 m^{-1}. Tillage directions were changed in steps of 5°, and slope gradients along the tillage direction varied from zero (contour tillage, along $\theta = 0°$ or $\theta = 180°$) to a maximum of 10% (up- and downslope tillage, $\theta = 90°$ or $\theta = 270°$).

Figure 10 shows how the direction of maximum soil displacement is rarely coincident with the direction of tillage, and how this deviation can change considerably depending on the type of tillage equipment (the α_2/α_1 ratio). For all curves, the coefficients that determine the influence of the slope gradient, β_1 and β_2, were set to 3.0 and 1.5 kg m^{-1} $\%^{-1}$ per tillage pass, respectively; α_1 was set to 50.0 kg m^{-1}, while the value of the α_2/α_1 ratio was changed to represent different implements. An implement that displaces a negligible net amount of soil laterally on a flat terrain has $\alpha_2 = 0$, while an

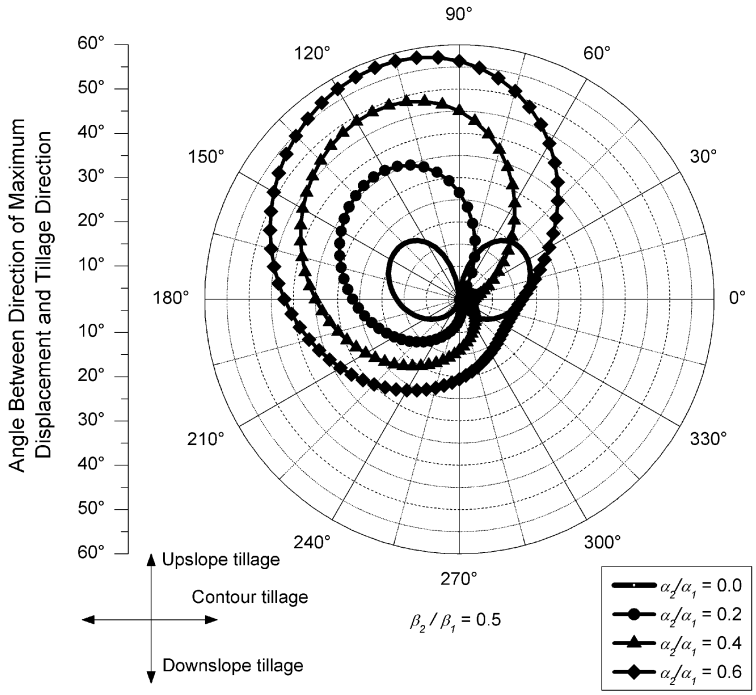

Figure 10. Angle between direction of maximum soil displacement and tillage direction ($\beta_2/\beta_1 = 0.5$, varying α_2/α_1 ratios).

implement with large lateral displacement has a higher α_2/α_1 ratio. Implements are assumed to displace soil laterally to left. Figure 10 shows that for an implement with zero net lateral displacement ($\alpha_2 = 0$) and for up- or downslope tillage, the maximum soil displacement coincides with the tillage direction. When tillage direction is slanted, lateral displacement due to gravity causes soil to be displaced at an angle with respect to the tillage direction, resulting in the double-circle pattern seen in the figure. For other implements, there is always a net lateral displacement of soil ($\alpha_2 \neq 0$), and the direction of maximum soil displacement rarely coincides with the direction of tillage. This deviation is greater for implements with large lateral displacements. The largest deviations occur when the tractor moves uphill (travel direction 120˚, for example) and the net displacement is larger to the left due to the slope gradients in that direction. In this case, the soil is displaced to the left of the tillage direction, at an angle that can be greater than 50˚. The results in figure 10 reflect the steepness (in the tillage and lateral directions) estimated at point *P* and the erosivity of the tillage implement represented by coefficients α_1, α_2, β_1, and β_2, and are independent of the terrain concavity. However, net erosion or deposition per tillage pass is determined by how the slope gradient varies in the landscape, that is, it is determined by the terrain curvature (concavity or convexity).

Figure 11 illustrates the fact that net erosion and deposition are functions of slope curvature, and their magnitudes depend on the relative orientation of the tillage implement with the terrain slope. One curve shows total soil translocation (caused by displacements in the tillage direction and perpendicular to it) computed every 5˚, normalized by the maximum translocation value (T/T_{max}). The second curve shows how erosion varies according to the tillage direction (E/E_{max}). The curves are based on computations for a tillage implement with translocation coefficients per tillage pass of $\alpha_1 = 50$ kg m^{-1}, $\alpha_2 = 25$ kg m^{-1}, $\beta_1 = 3.0$ kg m^{-1} %$^{-1}$, and $\beta_2 = 1.5$ kg m^{-1} %$^{-1}$. The asymmetry of the T/T_{max} curve is determined by the relative magnitude of the translocation factors α and β coupled with the tillage direction, which determines the effective slope gradients in the forward and lateral directions. The T/T_{max} curve would change somewhat if these coefficients were different, but would be essentially similar in shape to the curve plotted in the figure, with the greatest displacement occurring when tillage takes place in the downhill direction.

The same implement traversing the field in different directions produces different amounts of erosion or deposition. The largest net erosion or deposition does not necessarily occur for the same direction as maximum translocation. Here, it occurs along the path with the largest slope curvature; for the test field, it coincides with the *y*-direction ($\theta = 90^\circ$ or 270°). Minimum erosion occurs when tillage is performed on contour. Coefficients α_1 and α_2 do not affect the amount of deposition or erosion computed for the cell, which is controlled by the surface curvature and the coefficients related to the slope gradient (β_1 and β_2). Note, however, that the curve is symmetric: if the path is reversed, along any direction, the net erosion or deposition is the same. This occurs for up- and downslope tillage, as well as for contour tillage or any other direction in between. It is important to highlight the fact that this perfect symmetry in the computed erosion values derives from the fact that the soil translocation is assumed to be a linear function of the terrain slope gradient. If another relationship were used, the results would be different.

Figure 12 shows how the magnitude of deposition changes as a function of tillage direction for four different implements. The maximum amount of deposition is determined by the values of β_1 and β_2, reflecting the terrain curvature, while the α coefficients do not affect the resulting deposition. Therefore, the shape of the E/E_{max} curves is characterized by different values of the ratio β_2/β_1. Even for

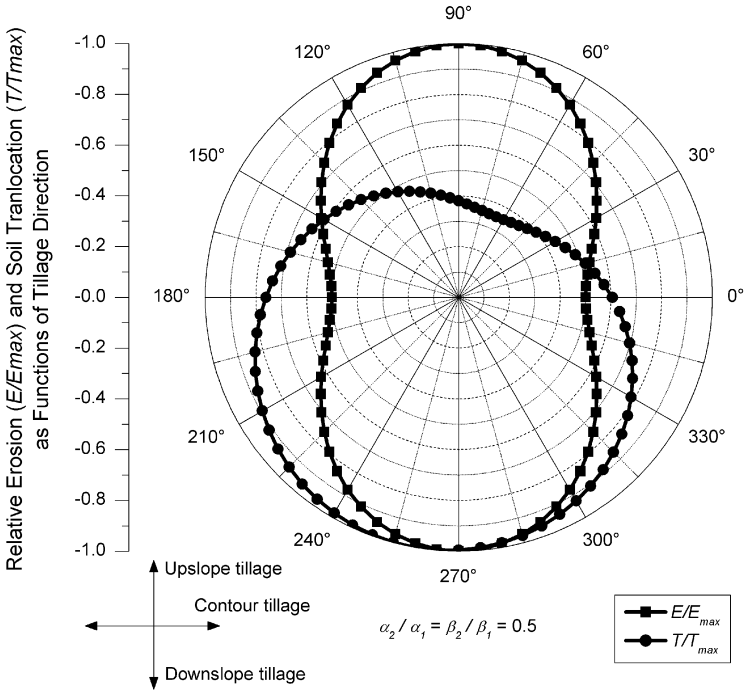

Figure 11. Relative soil translocation (T/T_{max}) and erosion (E/E_{max}) as functions of tillage direction.

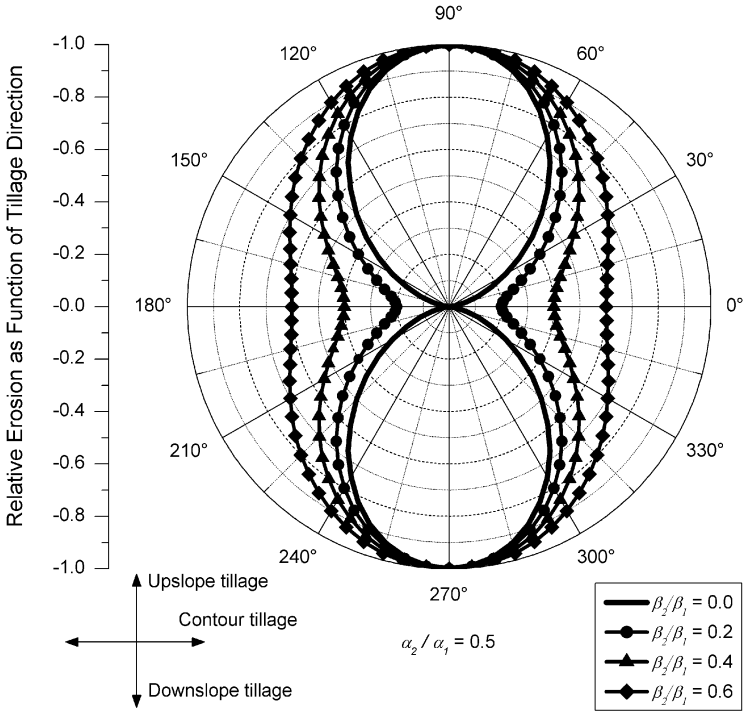

Figure 12. Relative erosion (E/E_{max}) as a function of tillage direction.

tillage on contour, deposition usually occurs because there is a net soil translocation in the lateral direction, resulting from the varying slope gradient, whose magnitude is controlled by coefficient β_2. In other words, with the passage of the implement, more soil is moved in the downhill direction for a pass in the upper part of the concave slope, where the slope is steeper, than for a pass at the lower part, where the slope is milder, creating a net transfer of soil that causes localized deposition. In the present test configuration, the maximum deposition always occurs for up- or downslope tillage, while the least erosion occurs for contour tillage. Deposition occurs because a concave slope configuration was used; the curves would be similar if the slope was convex, but instead of deposition, erosion would occur.

The changes in magnitude of soil translocation with tillage direction as depicted in this section are dependent on the model's assumption that the magnitude of soil translocation in the lateral direction is solely a function of the slope steepness in that direction, and it is independent of the slope steepness in the direction of tillage. Lobb and Kachanoski (1999), De Alba (2001), and Heckrath et al. (2006) suggested, based on experiments with moldboard plows, that soil displacement is best described by relationships using slope gradients in both tillage and lateral directions.

Modeling Tillage Erosion on Complex Landscapes

The newly developed model is used to predict erosion and deposition patterns caused by repeated tillage operations on a field of complex topography. The application serves to demonstrate the main capabilities of the computer model, and also to illustrate how different types of boundary conditions affect results and can be used to replicate phenomena that occur on a real tilled field. A 250 × 250 m field with a synthetic, undulating circular surface is used to define the landscape over which tillage takes place. The surface was generated using the curve:

$$z = 100.0 + 0.0002\left(x^2 + y^2\right)\sin\left(6\ \ \text{atan2}(x,y)\right) \quad (30)$$

where atan2(x,y) = $\tan^{-1}(y/x)$, but with a range of ($-\pi$,π). The surface is described by a grid of 5 m wide cells, and has terrain elevations in the range 75 to 125 m. Slope steepness varies from zero (horizontal) to 29.8%. Tillage is performed counterclockwise in a region defined by an annulus with inner and outer diameters of 25 m and 250 m, respectively. Tillage directions, shown by the arrows in figure 13, are parallel to the field borders. Because of the terrain configuration, slope steepness varies continuously, both in the direction of tillage and in the direction perpendicular to it. For this demonstration, an implement similar to a one-sided moldboard plow, with net lateral soil displacement to the right, is used. Soil translocation coefficients were α_1 = 50 kg m^{-1} pass^{-1}, α_2 = 25 kg m^{-1} pass^{-1}, β_1 = 3.0 kg m^{-1} %$^{-1}$ pass^{-1}, and β_2 = 1.5 kg m^{-1} %$^{-1}$ pass^{-1}. Soil bulk density was 1500 kg m^{-3}, and the simulation domain had a total of 7756 cells.

Two different simulations (A and B) were performed for the same terrain and tillage setup, but with different boundary conditions. Test A was simulated using the "open" boundary ($\partial\phi/\partial_{\vec{n}} = 0$), which lets soil flow in or out of the simulation domain. This condition, used to simulate tillage that extends beyond the model boundaries, does not let the presence of the boundary influence the soil movement inside the simulated region. It can be used when the location where tillage starts and stops is unknown or when it varies between operations. There is no localized erosion or deposition near the boundaries when this type of boundary condition is used. The field borders of test B, however, do not let any soil leave the

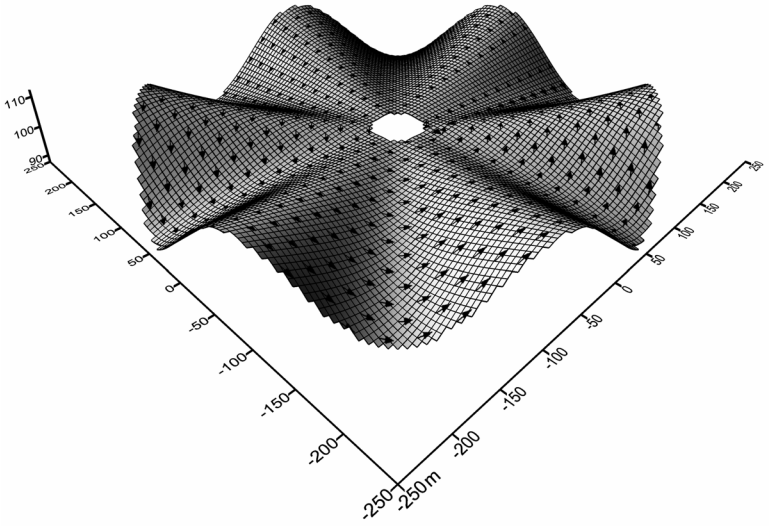

Figure 13. Initial terrain configuration and tillage directions.

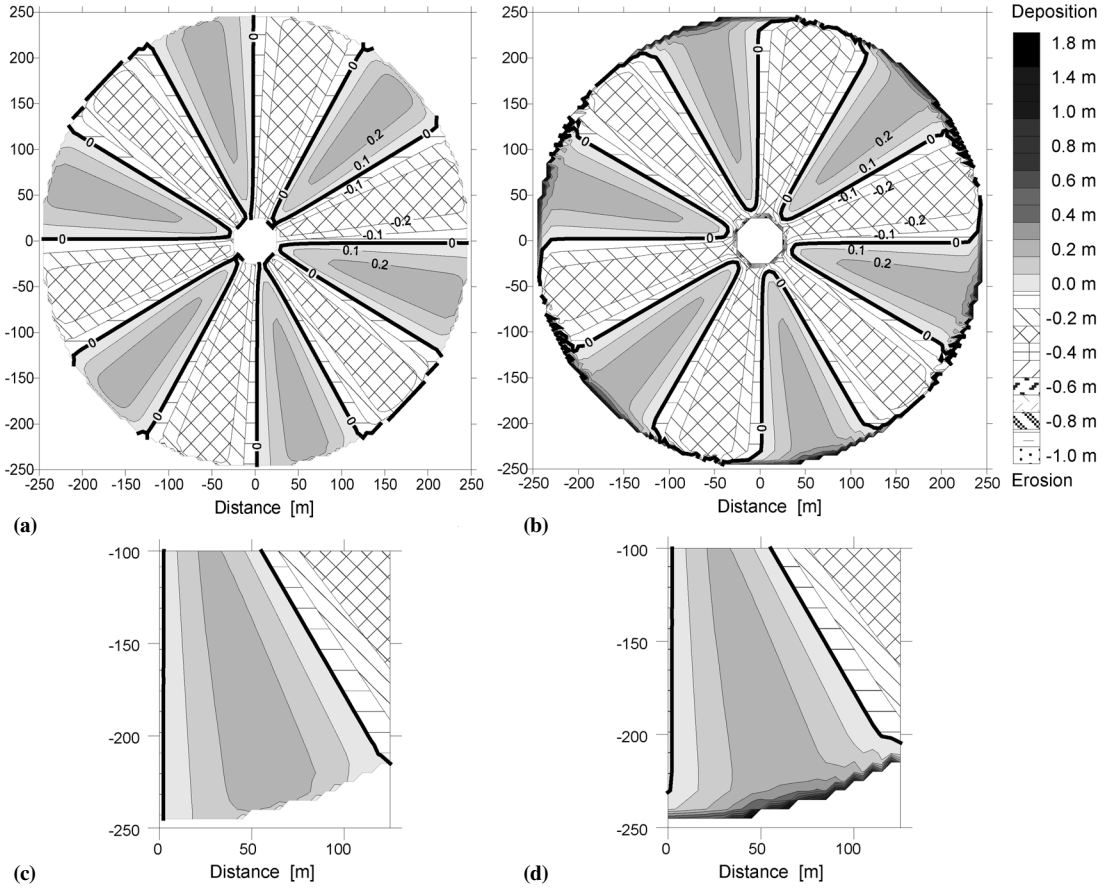

Figure 14. Erosion and deposition patterns after 200 tillage passes: (a) simulation with open boundaries; (b) simulation with closed boundaries; (c) detail, simulation with open boundaries; and (d) detail, simulation with closed boundaries.

field. This situation is enforced using the "closed" boundary type, which sets the soil flux normal to the boundary to zero ($\phi_{\vec{n}} = 0$).

Figure 14 shows the erosion and accumulation patterns after 200 tillage passes for both tests. Tillage caused erosion of the upper, convex areas, while accumulation occurred in the concave areas, resulting in decreased slope steepness. Areas mid-slope showed little net deposition or erosion. The influence of the closed boundaries used in test B (fig. 14b) can be seen especially near the outer perimeter. Substantial deposition occurred in the depressions, with the highest deposition amounts located just next to the field border. Near the inner border, erosion occurred as the tillage implement moved soil away from the border. In contrast, when an open boundary condition is prescribed where tillage moves soil away from the boundary (test A), there is an assumed soil flux

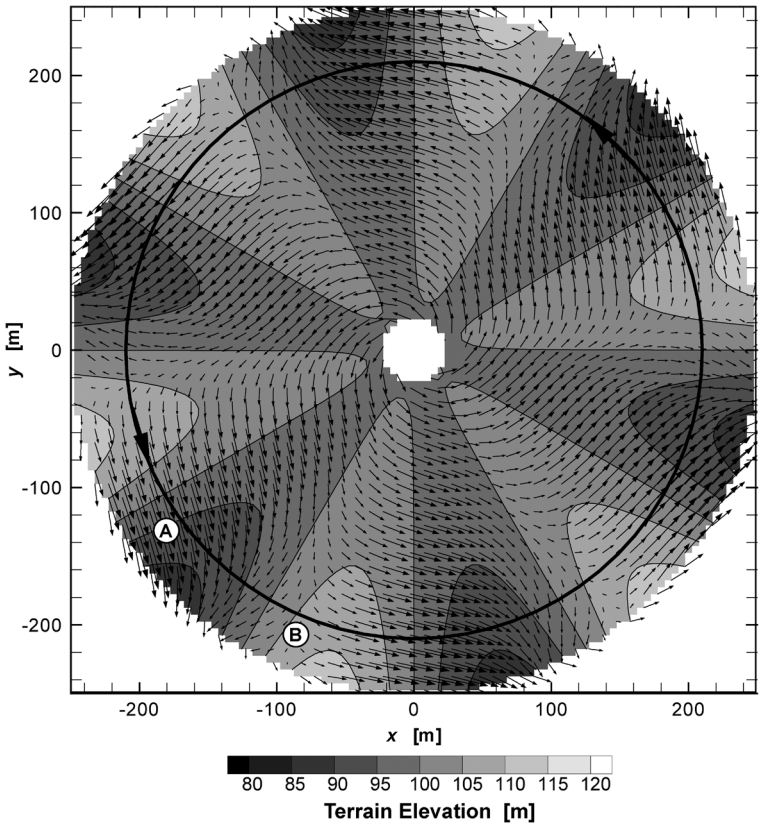

Figure 15. Soil flux vectors and terrain elevation after the 200th tillage pass, for the test case with open boundaries (test A). The dark areas indicate lower elevations (depressions), while light areas indicate regions of higher elevation. The black circular line indicates the tillage path used in figure 16.

that enters the simulation domain and balances the soil movement toward the domain's interior. This balance occurs only in the direction perpendicular to the boundary. The elevation of cells along the boundary still can change due to varying soil displacements along the tillage path.

Figure 15 shows the soil flux vectors, computed at the 200th pass for test A. Due to the combined effect of a tillage implement with high rate of lateral displacement, and the topography, which sloped in the radial direction, the direction of the resulting soil flux had a large deviation from the tillage direction, especially near the depressions at the outer rim of the tillage area, shown in the figure as darker shades of gray. The largest soil translocations occur when the implement is moving downslope toward the depressions (location A in fig. 15), which are gradually filled as soil moves in, although for test A, part of if leaves the domain through the outer boundary due to displacements perpendicular to the direction of tillage. In the same area, one can see that the soil translocation is practically perpendicular to the tillage direction when the implement is moving uphill at approximately 24% steepness (location B in the same figure). The forward soil translocation created by the tillage implemented is compensated by a downslope soil movement, so that the net soil movement is primarily the displacement in the lateral direction.

Figure 16 shows the initial terrain elevation and slope steepness, and the computed morphological changes after 100 and 200 passes along the tillage path with a radius of 210 m (shown in fig. 15) for test A. The results show that soil losses are greatest on the hilltops, and soil accumulation occurs at the base of the hillslopes. Because the domain is

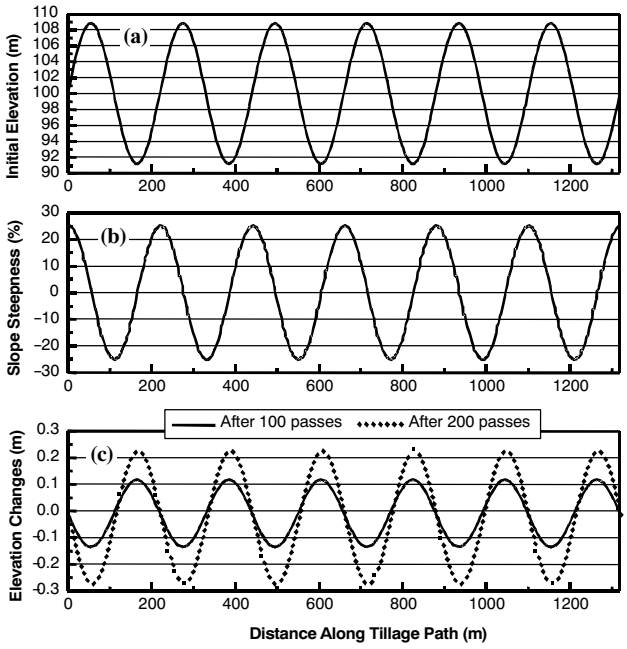

Figure 16. (a) Initial elevation, (b) initial slope steepness, and (c) computed erosion and deposition after 100 and 200 passes along a tillage path (radius = 210 m), for test A.

cyclic symmetric, the patterns are repeated. As this test uses the open boundary condition, soil enters the domain at the inner boundary and leaves through the outer boundary. The soil fluxes through these boundaries are controlled by the terrain slopes in the radial direction, which vary in both space

and time, as morphological changes take place. In the present test, more soil leaves the outer boundary than enters the inner boundary, resulting in a net soil loss for the entire field.

SUMMARY

A new model has been developed to predict erosion due to tillage operations in agricultural fields. Given initial terrain topography, tillage directions, and implement characteristics, the two-dimensional, grid-based model computes erosion and deposition after each tillage pass. GIS tools facilitate the specification of input data. Terrain elevations are given in the form a DEM, while tillage directions and the position of field boundaries are defined graphically. The model exploits the increased availability of high-resolution terrain elevation data derived from remotely sensed technologies, such as LiDAR (light detection and ranging). Higher spatial resolutions provide better estimations of slope gradients resulting from the interaction of tillage direction and topography, thereby improving the computation of tillage erosion. Higher resolutions also allow for greater flexibility in the placement of field borders, and linear features like vegetated strips and fences. Accurately located field borders, coupled with the ability to consider variable tillage directions, allow the simulation of contour tillage erosion, where tillage paths are usually curved.

The model determines morphological changes based on the spatial distribution of computed soil translocation within the field. Soil translocation is determined at the center of each cell as a function of implement type and size, operation characteristics, and orientation of the implement with respect to the local terrain. The model utilizes a linear relationship between soil translocation (in mass per tillage pass) and terrain slope steepness in the direction of tillage and in the direction perpendicular to it, as proposed by Lobb and Kachanoski (1999), assuming that orthogonal translocations can be determined independently. The magnitude of soil translocation is defined through empirical coefficients, whose values are derived from field observations and measurements. The coefficients represent tillage implement characteristics such as tool design and size, and operation parameters such as tillage speed and depth. Soil condition before tillage may also significantly influence the magnitude of soil translocation, as the degree of compaction, texture, cohesiveness, and the presence of roots affect how soil breaks into clods while being displaced by tillage tools. Because of altered cohesion, soil translocation in a field that has been recently tilled may be smaller than if the field has not been tilled in years. Similarly, translocation is expected to decrease with repeated tillage. In addition, for large, rigid-frame implements, each tillage tool may cause varying soil displacements as the implement weight interacts with an irregular soil surface. Although a large number of factors determine how soil translocation varies over irregular, complex terrain, the model's coefficients (α_1, β_1, α_2, β_2) can be calibrated to account for the most important factors and reproduce observed erosion patterns, thereby increasing the user's confidence in the predictive abilities of the model. A database of these coefficients can be found in the published literature, and recent experiments continue to expand it by including a wider variety of tillage implements (Van Muysen et al., 2006; Heckrath et al., 2006; Li et al., 2007b; Tiessen et al 2007a, 2007b, 2007c). There is some evidence that the lateral soil displacement may be correlated with the slope steepness in the direction of tillage (De Alba, 2001; Heckrath et al., 2006), or that translocation is not linearly related to slope steepness. The use of more complex expressions for determination of soil translocation would not require significant changes in the implementation of the mathematical model, but at present better relationships are not widely available for the most commonly used implements.

The application of the model to a problem for which an analytical solution is known demonstrated that the model equations are properly implemented and that the numerical solution is correct, stable, and accurate. Simulations indicate that the model is not particularly sensitive to grid cell sizes, and that it performs best when applied to grid sizes between 1.0 and 10 m. Fine meshes produce a better representation of the terrain topography, enhance the description of geometrically complex boundaries, and permit a better representation of the spatial variation of computed properties. In the simulation of boundary-induced erosion or deposition, where morphological changes gradually progress to the interior, grid sizes in the 1.0 to 5.0 m range are able to capture well the soil translocation changes that occur in the vicinity of boundaries, which in turn determine the net erosion or deposition rates. This range of mesh sizes usually exceeds the magnitude of soil displacements caused by tillage implements. The use of smaller mesh sizes is not recommended because it can lead to the computation of unrealistic and excessive elevation changes near closed boundaries.

Because tillage erosion is a function of the terrain's slope curvature, it is important to estimate slope gradients accurately. The method chosen (Horn, 1981) is considered one of the best when applied to natural terrains (Jones, 1998a). The nature of the method, which utilizes a 3×3 kernel, minimizes the effects of measuring errors commonly found in DEMs. When the method is applied to cells next to boundaries, interpolation is used to estimate terrain elevations for cells outside the simulation domain. The model does not require any special preprocessing such as smoothing of the initial terrain surface, and no other treatment is performed during the time-marching computations. The presence of boundaries does not have any negative impact on the solution, and the computed topography is smooth and free of oscillations.

Unlike models that are based on the diffusion analogy, the present model does not require tillage to be performed in alternating directions. The capability of simulating repeated operations in the same direction is particularly important near field borders; localized erosion occurs where tillage starts, and soil accumulation takes place where the implement is disengaged from the ground. The model's stability and computational efficiency; its ability to simulate tillage erosion in fields with complex boundaries, varying tillage directions, and realistic management sequences; and its convenient integration with GIS environments allow its use as a practical tool in a comprehensive conservation planning and management system.

REFERENCES

Boyce, W. E., and R. C. DiPrima. 1977. *Elementary Differential Equations and Boundary Value Problems.* 3rd ed. New York, N.Y.: Wiley.

Burrough, P. A., and R. A. McDonnell. 1998. *Principles of Geographical Information Systems.* Oxford, U.K.: Oxford University Press.

Dabney, S. M. 2006. Tillage erosion: Terrace relationships. In *Encyclopedia of Soil Science*, 1(1): 1752-1754. R. Lal, ed. New York, N.Y.: Marcel Dekker.

Dabney, S. M., Z. Liu, M. Lane, J. Douglas, J. Zhu, and D. C. Flanagan. 1999. Landscape benching from tillage erosion between grass hedges. *Soil Tillage Res.* 51(3-4): 219-231.

Da Silva, J. R. M., J. M. C. N. Soares, and D. L. Karlen. 2004. Implement and soil condition effects on tillage-induced erosion. *Soil Tillage Res.* 78(2): 207-216.

De Alba, S. 2001. Modeling the effects of complex topography and patterns of tillage on soil translocation by tillage with mouldboard plough. *J. Soil Water Cons.* 56(4): 335-345.

De Alba, S. 2003. Simulating long-term soil redistribution generated by different patterns of mouldboard ploughing in landscapes of complex topography. *Soil Tillage Res.* 71(1): 71-86.

Ferziger, J. H., and M. Perić. 1999. *Computational Methods for Fluid Dynamics.* 2nd ed. Berlin, Germany: Springer Verlag.

Fleming, M. D., and R. M. Hoffer. 1979. Machine processing of Landsat MSS data and DMA topographic data for forest cover type mapping. LARS Technical Report 062879. West Lafayette, Ind.: Purdue University, Laboratory for Applications of Remote Sensing.

Govers, G., K. Vandaele, P. Desmet, J. Poesen, and K. Bunte. 1994. The role of tillage in soil redistribution on hillslopes. *European J. Soil Sci.* 45(4): 469-478.

Heckrath, G., U. Halekoh, J. Djurhuus, and G. Govers. 2006. The effect of tillage direction on soil redistribution by mouldboard ploughing on complex slopes. *Soil Tillage Res.* 88(1-2): 225-241.

Horn, B. K. P. 1981. Hill shading and the reflectance map. *Proc. IEEE* 69: 14-47.

Jones, K. H. 1998a. A comparison of algorithms used to compute hill slope as a property of the DEM. *Computers and Geosci.* 24(4): 315-323.

Jones, K. H. 1998b. A comparison of two approaches to ranking algorithms used to compute hill slopes. *GeoInformatica* 2(3): 235-256.

Li, S., D. A. Lobb, M. J. Lindstrom, and A. Farenhorst. 2007a. Tillage and water erosion on different landscapes in the northern North American Great Plains evaluated using 137Cs technique and soil erosion models. *Catena* 70(3): 493-505.

Li, S., D. A. Lobb, and M. J. Lindstrom. 2007b. Tillage translocation and tillage erosion in cereal-based production in Manitoba, Canada. *Soil Tillage Res.* 94(1): 164-182.

Li, S., D. A. Lobb, M. J. Lindstrom, S. K. Papiernik, and A. Farenhorst. 2008. Modeling tillage-induced redistribution of soil mass and its constituents within different landscapes. *SSSA J.* 72(1): 167-179.

Lindstrom, M. J., W. W. Nelson, T. E. Schumacher, and G. D. Lemme. 1990. Soil movement by tillage as affected by slope. *Soil Tillage Res.* 17(3-4): 255-264.

Lindstrom, M. J., W. W. Nelson, and T. E. Schumacher. 1992. Quantifying tillage erosion rates due to moldboard plowing. *Soil Tillage Res.* 24(3): 243-255.

Lindstrom, M. J., J. A. Schumacher, and T. E. Schumacher. 2000. TEP: A tillage erosion prediction model to calculate soil translocation rates from tillage. *J. Soil Water Cons.* 55(1): 105-108.

Lobb, D. A., and R. G. Kachanoski. 1999. Modelling tillage erosion in the topographically complex landscapes of southwestern Ontario, Canada. *Soil Tillage Res.* 51(3-4): 261-277.

Lobb, D. A., R. G. Kachanoski, and M. H. Miller. 1995. Tillage translocation and tillage erosion of shoulder slope landscape positions measured using 137Cs as a tracer. *Canadian J. Soil Sci.* 75(2): 211-218.

Lobb, D. A., R. G. Kachanoski, and M. H. Miller. 1999. Tillage translocation and tillage erosion in the complex upland landscapes of southwestern Ontario, Canada. *Soil Tillage Res.* 51(3-4): 189-20.

Mech, S. J., and G. A. Free. 1942. Movement of soil during tillage operations. *Agric. Eng.* 23(12): 379-382.

Papendick, R. I., and D. E. Miller. 1977. Conservation tillage in the Pacific Northwest. *J. Soil Water Cons.* 32(1): 49-56.

Papiernik, S. K., M. J. Lindstrom, J. A. Schumacher, A. Farenhorst, K. D. Stephens, T. E. Schumacher, and D. A. Lobb. 2005. Variation in soil properties and crop yield across an eroded prairie landscape. *J. Soil Water Cons.* 60(6): 388-395.

Poesen, J., B. Van Wesemael, G. Govers, J. Martinez-Fernandez, P. Desmet, K. Vandaele, T. Quine, and G. Degraer. 1997. Patterns of rock fragment cover generated by tillage erosion. *Geomorphology* 18(3-4): 183-197.

Quine, T. A., and Y. Zhang. 2004. Re-defining tillage erosion: Quantifying intensity-direction relationships for complex terrain: 1. Derivation of an adirectional soil transport coefficient. *Soil Use and Mgmt.* 20(2): 114-123.

Ritter, P. 1987. Vector-based slope and aspect generation algorithm. *Photogrammetric Eng. and Remote Sensing* 53(8): 1109-1111.

Schneider, P., and D. Eberly. 2002. *Geometric Tools for Computer Graphics.* San Francisco, Cal.: Morgan Kaufman.

Schumacher, T. E., M. J. Lindstrom, J. A. Schumacher, and G. D. Lemme. 1999. Modeling spatial variation in productivity due to tillage and water erosion. *Soil Tillage Res.* 51(3-4): 331-339.

Sharpnack, D. A., and G. Akin. 1969. An algorithm for computing slope and aspect from elevations. *Photogrammetric Eng.* 35(3): 247-248.

Sibbesen, E. 1986. Soil movement in long-term field experiments. *Plant and Soil* 91(1): 73-85.

Sibbesen, E., C. E. Andersen, S. Andersen, and M. Flensted-Jensen. 1985. Soil movement in long-term field experiments as a result of cultivations: I. A model for approximating soil movement in one horizontal dimension by repeated tillage. *Exp. Agric.* 21: 101-107.

Tang, G., M. Zhao, T. Li, Y. Liu, and T. Zhang. 2003. Simulation on slope uncertainty derived from DEMs at different resolution levels: A case study in the Loess Plateau. *J. Geogr. Sci.* 13(4): 387-394.

Tiessen, K. H. D., G. R. Mehuys, D. A. Lobb, and H. W. Rees. 2007a. Tillage erosion within potato production systems in Atlantic Canada: I. Measurement of tillage translocation by implements used in seedbed preparation. *Soil Tillage Res.* 95(1-2): 308-319.

Tiessen, K. H. D., D. A. Lobb, G. R. Mehuys, and H. W. Rees. 2007b. Tillage erosion within potato production in Atlantic Canada: II. Erosivity of primary and secondary tillage operations. *Soil Tillage Res.* 95(1-2): 320-331.

Tiessen, K. H. D., D. A. Lobb, G. R. Mehuys, and H. W. Rees. 2007c. Tillage translocation and tillage erosivity by planting, hilling, and harvesting operations common to potato production in Atlantic Canada. *Soil Tillage Res.* 97(2): 123-139.

Van Muysen, W., and G. Govers. 2002. Soil displacement and tillage erosion during secondary tillage operations: The case of rotary harrow and seeding equipment. *Soil Tillage Res.* 65(2): 185-191.

Van Muysen, W., G. Govers, K. Van Oost, and A. Van Rompaey. 2000. The effect of tillage depth, tillage speed, and soil condition on chisel tillage erosivity. *J. Soil Water Cons.* 55(3): 355-364.

Van Muysen, W., G. Govers, and K. Van Oost. 2002. Identification of important factors in the process of tillage erosion: The case of mouldboard tillage. *Soil Tillage Res.* 65(1): 77-93.

Van Muysen, W., K. Van Oost, and G. Govers. 2006. Soil translocation resulting from multiple passes of tillage under normal field operating conditions. *Soil Tillage Res.* 87(2): 218-230.

Van Oost, K., G. Govers, and P. Desmet. 2000a. Evaluating the effects of changes in landscape structure on soil erosion by water and tillage. *Landscape Ecology* 15(6): 577-589.

Van Oost, K., G. Govers, W. Van Muysen, and T. A. Quine. 2000b. Modeling translocation and dispersion of soil constituents by tillage on sloping land. *SSSA J.* 64(5): 1733-173.

Van Oost, K., G. Govers, W. Van Muysen, and J. Nachtergaele. 2003. Modelling water and tillage erosion using spatially distributed models. In *Long-Term Hillslope and Fluvial System Modeling*, 101-122. A. Lang, K. Hennrich, and R. Dikau, eds. Heidelberg: Springer Verlag.

NOMENCLATURE

A = azimuth; surface area of a control volume
a = regression coefficient; soil translocation when slope is zero
b = regression coefficient in soil translocation distance – slope gradient relationship
CV = control volume
D = tillage depth (thickness of the plow layer)
d = soil translocation distance of the plow layer
d_{DN} = soil translocation distance for tillage in the downslope direction
d_{UP} = soil translocation distance for tillage in the upslope direction
dS = infinitesimal control surface
dV = infinitesimal control volume
E = computational node to the east (subscript); tillage erosion (mass per unit area)
e = east face of a control volume (subscript)
i, j = grid number along x and ydirections
$\vec{i}, \vec{j}$ = unit vectors along x and y directions
k = tillage erosion coefficient
K = tillage erosivity expressed as a diffusion coefficient
M = soil mass
N = computational node to the north (subscript)
n = north face of a control volume (subscript); time integration level (superscript)
$\vec{n}$ = vector normal to a surface
P = computational node at the center of a control volume
Q_s = soil mass flux (mass per unit width per tillage operation)
Q_{DN} = soil mass flux in the downslope direction
Q_{UP} = soil mass flux in the upslope direction
r = tillage direction
S = terrain slope gradient in percentage; computational node to the south (subscript)
s = terrain slope gradient; south face of a control volume (subscript)
T = soil translocation due to tillage erosion
t = time
$\vec{t}$ = unit vector defining a tillage direction
$\vec{v}$ = soil displacement velocity
W = computational node to the west (subscript)
w = west face of a control volume (subscript)
x = Cartesian direction or axis
y = Cartesian direction or axis
z = Cartesian direction or axis; terrain elevation
α = soil translocation amount for level land
β = soil translocation coefficient related to slope gradient
γ = soil translocation coefficient related to slope curvature
$\Delta x, \Delta y$ = cell sizes in the x and y directions
Δz = change in terrain elevation
Φ_i = soil mass flux in units of mass per tillage operation
ϕ_i = soil mass flow rate per unit width per tillage operation
θ = direction angle measured counterclockwise from the east
ρ_b = soil bulk density
1 = refers to tillage direction (subscript)
2 = refers to direction perpendicular to tillage direction (subscript)